Ecological Modelling 415 (2020) 108835

Contents lists available at ScienceDirect

Ecological Modelling

journal homepage: www.elsevier.com/locate/ecolmodel

Automatic calibration and improvements on an instream chlorophyll *a* simulation in the HSPF model

Dong Hoon Lee[a], Jin Hwi Kim[a], Mi-Hyun Park[b], Michael K. Stenstrom[b], Joo-Hyon Kang[a,*]

[a] Department of Civil and Environmental Engineering, Dongguk University-Seoul, Seoul 04620, South Korea
[b] Department of Civil and Environmental Engineering, University of California-Los Angeles 90095, USA

ARTICLE INFO

Keywords:
Chlorophyll *a*(chl *a*)
Phytoplankton
Algae
Hydrological simulation program-fortran (HSPF)
Automatic calibration
Sensitivity analysis

ABSTRACT

Accurate prediction of chlorophyll *a* (Chl *a*) concentration in surface water bodies such as lakes or rivers is crucial for water quality management. This study improved the predictive simulation of instream Chl *a* with the Hydrological Simulation Program-FORTRAN (HSPF) by adding automatic calibration and modifying the growth-temperature formulation of phytoplankton in the original HSPF model. A total of 62 model parameters, selected from a series of sensitivity analyses, were automatically calibrated in a stepwise manner for different variables in the order of flow, sediment, water temperature, ammonia/nitrate couple, and phosphate/Chl *a* couple. With finer temporal resolution (5–8 days) data than those of majority of the existing HSPF studies, the automatic calibration procedure provided the model with performance ratings of 'satisfactory' or better for all the variables including nutrients and Chl *a*: The percent bias values ranged from -18% - 54% and -20% – 62% for nutrients and Chl *a*, respectively. The original linear equation on the growth-temperature relationship of phytoplankton in simulating instream Chl *a* was modified using a quadratic equation and an exponential equation. The exponential equation outperformed the original linear and quadratic equations, particularly in simulating the excess concentrations of Chl *a* observed during summer seasons. For the validation data set, the exponential equation predicted 78% of the eutrophic cases while the linear and quadratic equation only predicted 53% and 13% of the eutrophic cases, respectively. The modified HSPF model offers an improved prediction of instream Chl *a*. This approach will be useful for providing early warning of algal blooms, facilitating the implementation of effective management of stream water quality.

1. Introduction

Chlorophyll *a* (Chl *a*) is a simple and easy-to-measure indicator of the phytoplankton biomass in a water body, and thus has long been used as a key water quality parameter for determining the trophic state of a water body (Boyer et al., 2009; Hutorowicz and Pasztaleniec, 2014; Paerl et al., 2003). Although the level of Chl *a* in a water body is a reflection of complicated interactions among various internal and external conditions of that water body including hydrological, geological, physicochemical, and meteorological factors, a high concentration of Chl *a* is generally considered a symptom of water quality degradation due to excess nutrient inputs (Smith et al., 1999; Lee et al., 2011).

Predictive simulation or forecasting of Chl *a* concentration in a surface water body such as a lake or a stream has recently become an important task for water quality managers to ensure early warning of algal blooms in a water body. It is also important in the development of a proactive management plan to counter eutrophication (Lee et al., 2005; Wagner and Erickson, 2017). However, the interactions among the various environmental factors and their influences on the level of Chl *a* can be very complicated and thus accurate prediction of Chl *a* concentration remains a challenging task.

With rapidly advancing computer techniques and the development of model theories, water quality models have become effective tools for predicting or forecasting water quality, with their ability to simulate the transport of pollutants and their interactions with various environmental factors (Tim, 1995; Loucks and Van Beek, 2005). Most water quality models adopt numerical approaches to solve sets of differential equations that describe the underlying mechanisms and processes associated with pollutant fate and transport in and between the system components.

Various water quality models have been developed to date for different types of water bodies with different spatial and time scales. Among these models, watershed models have a broad applicability to water resources and quality management because they can provide an

* Corresponding author.
E-mail address: joohyon@dongguk.edu (J.-H. Kang).

https://doi.org/10.1016/j.ecolmodel.2019.108835
Received 1 May 2019; Received in revised form 31 August 2019; Accepted 2 October 2019

integrated knowledge of hydrological, biological, and physicochemical interactions within and among different watershed components such as surface waters, ground waters and soil; point and distributed pollutant sources (Singh and Frevert, 2006). For the past few decades, watershed models have thus been widely used, particularly for developing total maximum daily loads (TMDLs), targeting different water quality parameters depending on their site-specific significance (Jha et al., 2010; Chen et al., 2011; Sherk and Linker, 2013). For example, eutrophication has been of great concern for surface water bodies such as streams and lakes. The use of an appropriate watershed model enables direct estimation of the quantitative interactions between nutrient loads from catchments and phytoplankton growth (typically represented by Chl *a*) in nested water bodies, rendering the model a useful decision-making tool (Auer et al., 1986; Debela et al., 2006).

The Hydrological Simulation Program-FORTRAN (HSPF) is one of the most comprehensive watershed models that is widely used in support of various regulatory and planning applications worldwide (Alberk et al., 2004; Fonseca et al., 2014). HSPF performs the integrated simulation of the surface, soil, and stream processes of hydrology, hydraulics, and water quality driven by continuous and dynamic storm events, as well as the sources of point and nonpoint pollutants in a watershed. Its flexibility on various regional scales and land use types, including urban and non-urban land uses, has rendered this model widely applicable (Bicknell et al., 2001). In HSPF, a single lumped sum phytoplankton parameter is considered for calculating algal biomass. The result is then transformed to a Chl *a* concentration using an empirical Chl *a*/biomass ratio (Bicknell et al., 2001; USEPA, 2013). HSPF uses Monod kinetics to calculate the phytoplankton growth rate, incorporating various limiting factors such as nutrient concentrations, light intensity, including attenuation with water depth, self-shading effect, and water temperature. Although the phytoplankton calculation module of HSPF is sophisticated enough to consider most of the well-known limiting factors in many situations, it can be further refined to increase the accuracy of Chl *a* simulation. The current version of HSPF (HSPF12) assumes that the maximum growth rate of the phytoplankton linearly increases as the water temperature increases, until being retarded from a specific water temperature up to the upper temperature limit. If the water temperature is outside of the lower or upper limits of the water temperature assigned by the users, the growth is assumed to have ceased (Bicknell et al., 2001). However, according to the evidence found in many previous studies, an envelope curve of the maximum growth rate versus water temperature is more appropriate for predicting total algal biomass consisting of multiple phytoplankton species with different temperature preferences and growth rates, while the upper temperature limit for the growth termination can still be valid in a situation where the maximum water temperatures are above the optimum temperatures (Bowie et al., 2019).

Another critical issue for achieving accurate HSPF simulation is model calibration and validation. Most of the prior HSPF studies focused on lumped sum variables for organics or nutrients as their modeling targets such as biological oxygen demand (BOD), total nitrogen (TN), and total phosphorous (TP). However, studies on Chl *a* simulation are rare, probably due to the intrinsic difficulty in validating the model with its very large number of model parameters that must be estimated or calibrated for hydrology as well as the many interrelated water quality variables. Furthermore, while most previous HSPF studies reported acceptable accuracy of the simulation results based on monthly data or monthly averaged data, few studies have reported acceptable modeling accuracy based on data with a finer temporal resolution than months

This study focuses on improving the Chl *a* simulation accuracy with two approaches: 1) improvement of the model validity using an automatic calibration procedure and 2) refinement of the temperature-growth formulation of the phytoplankton to improve the Chl *a* simulation accuracy. The Seom watershed in Korea is used as an example but the procedure is generally applicable to other water bodies. We conducted a global sensitivity analysis to select the model parameters to be calibrated. The HSPF model was automatically calibrated for the flow rate, Chl *a*, and selected water quality variables most strongly related to phytoplankton growth, including ionic nutrient species, sediment, and water temperature. The formulation of the phytoplankton growth in the phytoplankton module of HSPF was modified using two different mathematical expressions (quadratic and exponential equations) to improve the Chl *a* predictability of the HSPF model. The model's validity was demonstrated using various indicator values of model accuracy.

The automatic calibration procedure demonstrated in this study and the resulting set of critical model parameters should be useful guidance for other site-specific applications of a sophisticated watershed model such as HSPF. Furthermore, the refined HSPF model with finely tuned model parameters will provide better forecasting or prediction of Chl *a*, supporting early warning techniques of algal blooms and allowing decision making for proactive algal management.

2. Methods

2.1. Study site description

The study area is the Seom Watershed of the South Han River basin, located in South Korea (Fig. 1). It includes 5 local administrative districts and two cities with a total population of 380,000 as of 2015. The area of the Seom Watershed is 1473.21 km^2 and the mean elevation is 308.15 m, with the average slope of 14.3°. The mainstream of the Seom Watershed is the Seom River with a length of 67.3 km, and discharges into the Han River. In this area, the annual average total precipitation is 1345 mm with over 65% of the total precipitation occurring from June to August. However, the total annual precipitation showed a decreasing trend during the study period (from 2188 mm in 2011 to 908 mm in 2015).

Table 1 shows the land use composition of the Seom Watershed, categorized into seven land use classes (urban, agricultural, forest, grassland, wetland, bare land, and water). The Seom Watershed is dominated by forest land use (75.63%) followed by the agricultural land use (17.21%), with only a relatively small fraction (3.65%) of urban land use. Therefore, the major nonpoint pollution sources are agricultural areas including crop lands and livestock farms. The agricultural land of the Seom Watershed has typically been used for crop and livestock farming. As of 2010, the total livestock number (cattle, pigs, and poultry) was 1,367,392, with a total livestock wastewater production of 5854.59 kg/day (Ministry of Environment, 2010, http://www.wamis.go.kr). The identified point sources of pollutants include effluents from six municipal tertiary wastewater treatment plants (treatment capacity > 500 m^3/d), 34 community wastewater treatment plants (treatment capacity ≤ 500 m^3/d), three agro-industrial wastewater treatment plants, one wastewater treatment plant from an industrial complex (mostly electronics and mechanic industries) and one livestock wastewater treatment plant.

2.2. HSPF model setup

2.2.1. HSPF model and data preparation

The main modeling components of HSPF are water quantity and quality processes on pervious land segment (PERLND) and impervious land segment (IMPLND), and free-flow reach or well-mixed reservoirs (RCHERS). Processes considered in the pervious land segment (PERLND) include water budget, snow melt, sediment production and removal, nitrogen and phosphorous behavior, and pesticide behavior. Major processes considered in the impervious land segment (IMPLND) are overland flow and pollutant wash off. The calculated water and constituents generated in the pervious and impervious land segments are transferred to the linked reach segments (RCHERS), where flow routing and transport simulations are conducted that involve various

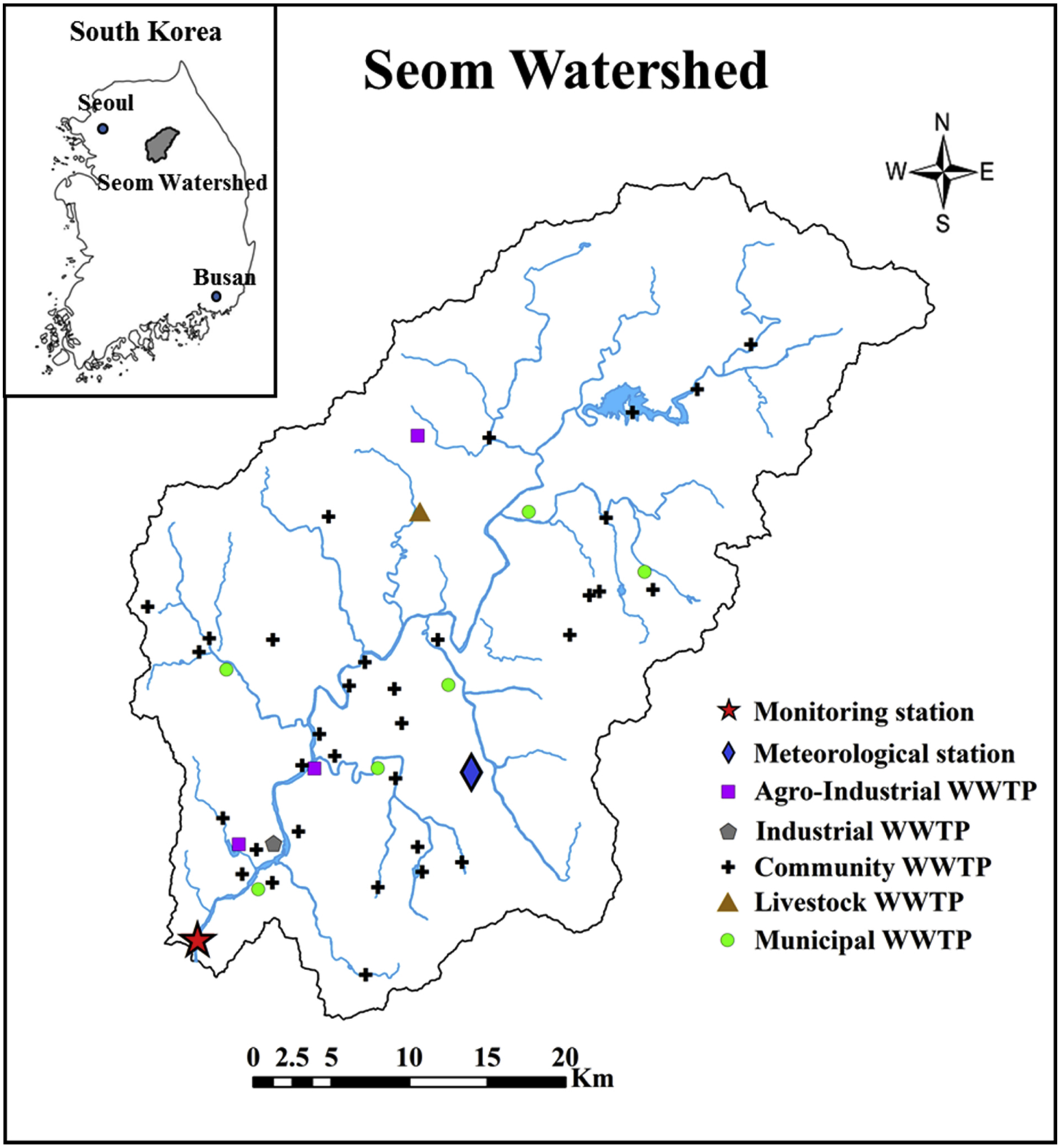

Fig. 1. Map of the Seom Watershed showing locations of point sources, the meteorological station, and the monitoring station.

physico-chemical parameters such as water temperature, dissolved oxygen, pH, inorganic carbon, alkalinity, organic and inorganic constituents (nitrogen and phosphorous), planktons, and their interactions with sediment and atmosphere. Fig. 2 shows the components of the HSPF model built up for the study area.

The data input to the model include meteorological data, spatial data, monitoring data, and point source data. The meteorological data include time series data of hourly rainfall, wind speed, solar radiation, cloud amount, due point, topsoil temperature, and daily minimum and maximum air temperatures, collected during the study period at the Wonju meteorological station located within the study area. The spatial data include the most recent versions of a 30 m x 30 m resolution digital elevation model (2014), and GIS layers of the watershed boundary (2014), stream network (2014), and land uses (2013), which were obtained from relevant governmental agencies. No profound changes in these spatial characteristics were reported during the study period. When constructing the model, the study area was divided into thirteen subwatersheds, based on the major tributaries (2nd order streams) of the Seom River (the main stream of the study area). Spatial analyses necessary for obtaining boundaries, areas, and average elevations of the subwatersheds were conducted using ArcGIS 10.0 (ESRI, California, USA). For the purpose of model calibration and validation, the water quality and flow rate data at the outlet point of the Seom Watershed were obtained from the Ministry of Environment (MOE), Korea. The flow rate data comprised the daily values of the river discharge; the water quality data included water temperature (TW), concentrations of Chl *a*, phosphate (PO_4^{3-}), nitrate (NO_3-), ammonium (NH_4^+), and suspended solids (SS) measured at intervals of 5–8 days. For the input point source data, daily flow rates and major pollutant concentrations (BOD, TN, TP, and SS) of the effluents from the wastewater treatment plants were obtained from MOE. The concentrations of NH_4^+, NO_3-, and PO_4^{3-} in the effluent were then estimated using the average

Table 1
Sensitivities and calibrated values of the model parameters selected for the model calibration with respect to hydrology, sediment, and water temperature.

Parameter			Description	Range		LH-OAT sensitivity to RMSE (S_{LH})			Calibrated value	Remarks
Group	Name	Unit		min	max	Flow rate	Sediment concentration	Water temperature		
Hydrology (10 parameters)										
PERLND	LZSN	in	Lower zone nominal storage	0.01	100	10.330	–	–	2.032	
PERLND	INFILT	in/hr	Index to the infiltration capacity of the soil	0.001	100	17.399	–	–	0.048	
PERLND	AGWRC	1/day	Basic groundwater recession rate	0.001	0.999	100.787	–	–	0.914	
PERLND	UZSN	in	Upper zone nominal storage	0.01	10	7.424	–	–	0.923	
PERLND	INTFW	–	Interflow inflow parameter	0	100	4.370	–	–	3.548	
PERLND	IRC	1/day	Under zero inflow; this is the ratio of today's interflow outflow rate to yesterday's interflow outflow rate	0.3	0.85	16.811	–	–	0.486	
PERLND	LZETP	–	Lower zone evapotranspiration parameter.	0	100	5.430	–	–	0.567	
PERLND	DEEPER	–	Fraction of groundwater inflow that will enter deep groundwater	0	1	8.211	–	–	0.291	
PERLND	BASETP	–	Fraction of remaining potential evapotranspiration that can be satisfied from baseflow if enough is available	0	1	1.056	–	–	0.118	
PERLND	AGWETP	–	Fraction of remaining potential evapotranspiration that can be satisfied from active groundwater storage if enough is available	0.001	0.999	0.308	–	–	0.054	
Sediment (14 parameters)										
PERLND	JRER	–	Exponent in the soil detachment equation	1.5	2.5	–	151.750	–	1.501	
PERLND	KSER	–	Coefficient in the detached sediment washoff equation	0.5	5	–	63.429	–	0.5-4.276	calibrated for each land-use class
PERLND	JSER	–	Exponent in the detached sediment washoff equation	1.5	2.5	–	257.991	–	2.5	
IMPLND	KEIM	–	Coefficient in the solids washoff equation	0.001	5	–	56.432	–	0.033	
IMPLND	JEIM	–	Exponent in the solids washoff equation	1	2.5	–	127.967	–	2.471	
IMPLND	ACCSDP	tons/ac/day	Rate at which solids accumulate on the land surface	2.5E-4	2	–	79.935	–	2.5E-4	
IMPLND	REMSDP	–	Fraction of solids storage that is removed each day	0	1	–	27.437	–	0.116	
RCHRES	POR	–	Porosity of the bed. Used to estimate bed depth	0.3	0.6	–	30.333	–	0.482	
RCHRES	KSAND	–	Coefficient in the sand load power function formula	0.01	20	–	6.898	–	0.526	
RCHRES	EXPSND	–	Exponent in the sand load power function formula	0.01	20	–	33.309	–	1.750	
RCHRES	TAUCS (for silt)	lb/ft^2	Critical bed shear stress for scour (less than or equal to TAUCS)	1.0E-7	0.5	–	28.179	–	1.0E-7	
RCHRES	M (for silt)	lb/ft^2·d	Erodibility coefficient of silt	0.01	20	–	16.259	–	14.492	
RCHRES	TAUCS (for clay)	lb/ft^2	Critical bed shear stress for scour of clay (less than or equal to TAUCS)	1.0E-7	0.5	–	10.980	–	1.0E-7	Smaller than or equal to the TAUCS value for silt
RCHRES	M (for clay)	lb/ft^2·d	Erodibility coefficient of clay	0.01	20	–	6.957	–	0.01	
Water temperature (6 parameter)										
RCHRES	CFSAEX	–	Correction factor for solar radiation	0.01	2	–	–	22.018	0.718	
RCHRES	KATRAD	–	Long wave radiation coefficient	1	20	–	–	46.069	12.032	
RCHRES	KCOND	–	Conduction-convection heat transport coefficient	1	20	–	–	10.853	20.000	
RCHRES	KEVAP	–	Evaporation coefficient	1	10	–	–	27.565	1.027	
RCHRES	TGRND	^{o}F	Temperature of ground if constant	14	113	–	–	211.669	34.419	
RCHRES	KMUD	kcal/m^2/^{o}C/hr	Heat conductance coefficient between water and the ground	0	100	–	–	49.359	3.398	

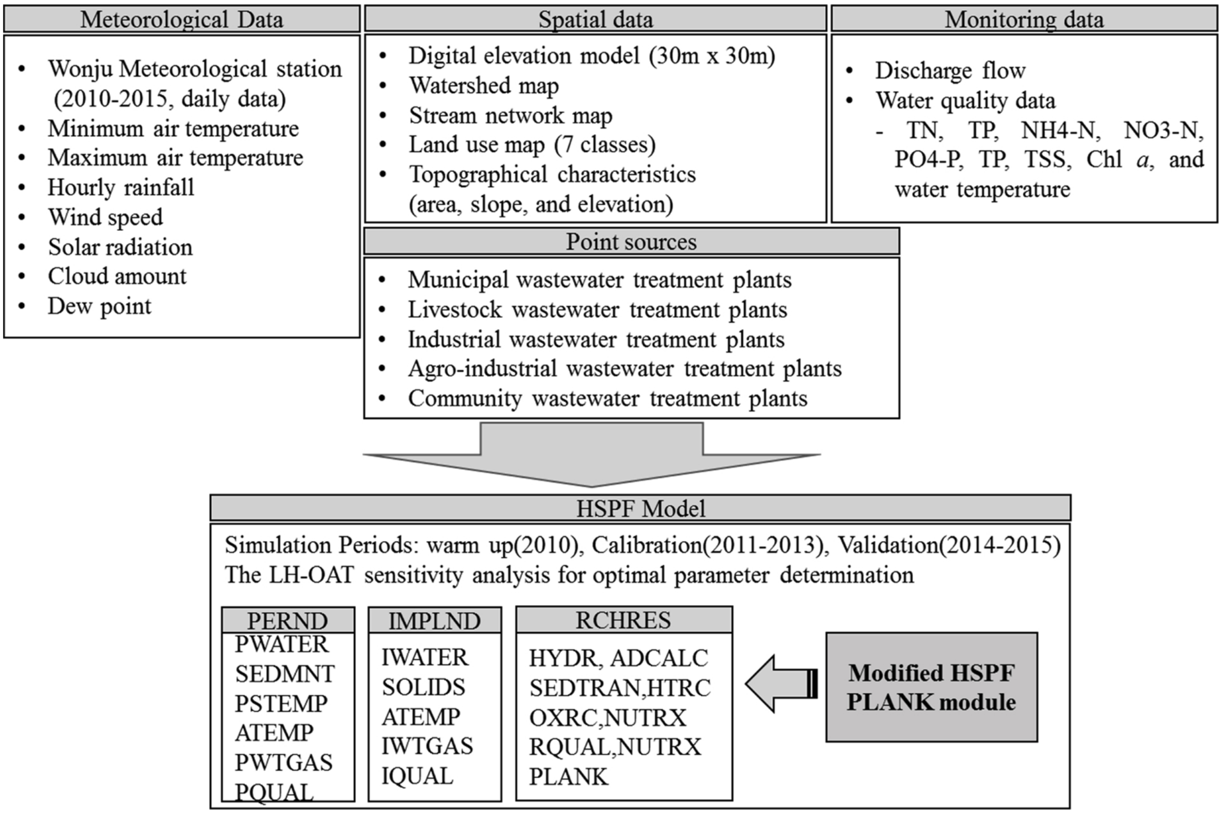

Fig. 2. Components of the HSPF model set up for the study area.

fractions of these species in TN and TP, as reported elsewhere (Kang et al., 2005; Park et al., 2013).

2.2.2. Modifications of the phytoplankton module

In HSPF, phytoplankton is simulated as a single lumped variable of many species, and the PLANK module simulates the core biological processes of the phytoplankton in the reach segment. In PLANK, the temperature dependency of the maximum growth rate of the phytoplankton is considered using a piecewise linear function as shown in Fig. 3. The piecewise linear function consists of a linear function with a positive slope between the lower temperature limit (TALGRL) and the optimal temperature (TALGRM), and a constant function between TALGRM and the upper temperature limit (TALGRH) to simulate the growth retardation in this higher temperature range. If the water temperature is below TALGRL or above TALGRH, the growth is assumed to cease completely.

In this study, the linear function defined between TALGRL and TALGRM was modified with two different curvilinear functions (i.e., quadratic and exponential), as illustrated in Fig. 3, and the accuracies of the Chl *a* prediction after the modifications were examined. A previous supporting hypothesis of this modification was that a curvilinear function might better represent the temperature-growth relationship of phytoplankton when many species are grouped together, in the simulation of total biomass (Bowie et al., 2019). We then compared the accuracies of the Chl *a* prediction for the following three formulations over the temperature range between TALGRL and TALGRM:

Linear (original equation): $\mathrm{TCMAL} = (\mathrm{TW} - \mathrm{TALGRL})/(\mathrm{TALGRM}\text{-}\mathrm{TALGRL})$ (1)

Quadratic: $\mathrm{TCMAL} = (\mathrm{TW}^2 - \mathrm{TALGRL}^2)/(\mathrm{TALGRM}^2\text{-}\mathrm{TALGRL}^2)$ (2)

Exponential: $\mathrm{TCMALG} = \{\exp(\mathrm{TW}) - \exp(\mathrm{TALGRL})\}/\{\exp(\mathrm{TALGRM}) - \exp(\mathrm{TALGRL})\}$ (3)

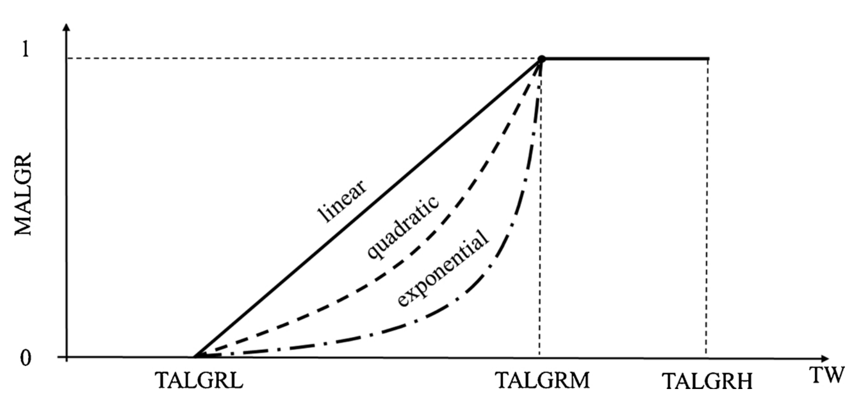

Fig. 3. Relationship between the maximum phytoplankton growth and water temperature in HSPF (linear equation is the original formulation, while quadratic and exponential equations are modifications in this study).

2.3. Sensitive analysis

A sensitivity analysis was performed using the Latin Hypercube-One factor at a Time (LH-OAT) method, which is known to be a cost-effective method in many water quality modeling applications (van Griensven et al., 2006; Park et al., 2014). The LH-OAT method is based on the Monte Carlo simulation but uses a stratified sampling technique for selecting the values of input parameters, called Latin Hypercube (LH) sampling, followed by the One factor at a Time (OAT) sampling. A number of random sets of the input parameters are sampled from the strata of evenly subdivided parameter hyperspace with an equal probability; the sample points are selected such that each interval of each input parameter is sampled only once (i.e., LH points). The method then operates a series of loops of model simulation by changing one parameter at a time (i.e., OAT sampling) around each Latin Hypercube (LH) point, and then computes the partial effect for each parameter and each LH point (Eq. (4)). The final effect of a parameter is calculated by averaging the partial effects over all LH points (Eq. (5)); as such, local sensitivities (i.e., partial effects) are integrated into a global sensitivity (i.e. final effect). The variance of the partial effects measures the existence of nonlinearity or correlations with other input parameters (van Griensven et al., 2006).

$$S_{i,j} = \left| \frac{100 \times \left(\frac{M(e_1, \ldots, e_i(1+f_i), \ldots, e_p) - M(e_1, \ldots, e_i, \ldots, e_p)}{[M(e_1, \ldots, e_i(1+f_i), \ldots, e_p) + M(e_1, \ldots, e_i, \ldots, e_p)]/2} \right)}{f_i} \right| \tag{4}$$

$$S_{LH,i} = \sum_{j=1}^{N} S_{i,j} \tag{5}$$

Where *M(·)* is the model function, $S_{i,j}$ is the partial effect of the parameter e^i for a given LH point, *j*, f_i is the changing fraction of the parameter e_i, whose sign is randomly defined, *N* is the total number of LH points, and $S_{LH,i}$ is the final sensitivity value for the parameter e_i.

Among the numerous hydrological parameters, a total of ten parameters, frequently reported in the literature as important parameters for flow calibration, were selected (US EPA, 2000; Abdulla et al., 2007; LaWare and Rifai, 2006). In contrast, sensitivity analyses for the model parameters associated with water quality were rarely conducted in previous HSPF modeling studies, and no published HSPF literature reporting the sensitivities of model parameters in relation to Chl *a* was found. Therefore, most of the model parameters associated with the water quality processes involved in the simulation mode of this HSPF modeling were considered. A total of 87 model parameters were thus considered in the sensitivity analysis including the parameters associated with hydrology, sediment, TW, two nitrogen species (NH_4^+ and NO_3^-), PO_4^{3-}, and Chl *a*. Ammonia can be transformed into nitrate by nitrification under oxidizing condition, and thus sensitivities of the model parameters for the ammonia processes to the nitrate concentration were also investigated. Similarly, mutual sensitivities of the parameters for phosphate and phytoplankton on the concentrations of PO_4-P and Chl *a* were examined because phosphate is a critical limiting factor of phytoplankton growth, A full list of the model parameters and their ranges used for the sensitivity analysis are provided in Supplementary Materials (Table S1-5).

The root-mean-square-errors (RMSE) between the observed and simulated values of flow rate, or target water quality variables at the outlet point of the study watershed, were used as the model function for the sensitivity calculation. For each model parameter, 50 LH points with four different changing fractions for the model parameters (changing fraction, f = 0.05, 0.10, 0.15, and 0.20) were evaluated to determine the sensitivities of the model, which were then averaged over the four fractions for the sensitivity ranking of the model parameters. The repeated running of HSPF with varying model parameter values required for the sensitivity analysis was automated by implementing the LH-OAT algorithm in MATLAB R2017a (Mathworks, Massachusetts, USA) linked with HSPF.

2.4. Model calibration and validation

The model was run for six years from Jan 2010 to Dec 2015, consisting of warmup (2010), calibration (2011–2013), and validation periods (2014–2015). The ten hydrological parameters as well as the impervious fractions of the respective six land use classes (excluding water land use) —urban, agricultural, forest, grassland, wetland, and bare land— were calibrated with respect to the measured flow data. Among the model parameters of water quality processes, those that can be estimated by topographical and meteorological information were fixed. To select the parameters of water quality processes for calibration, the results of the sensitivity analysis were referenced. Model parameters with a LH-OAT sensitivity value (S_{LH}) smaller than 0.1 were considered as insensitive and excluded in the calibration.

The model was calibrated in a stepwise manner as follows. The model was first calibrated for the flow rate followed by sediment, TW, NH_4^+/NO_3^- couple, and PO_4^{3-}/Chl *a* couple, in order. In each calibration for the flow rate, sediment, and TW, the relevant model parameters were optimized by minimizing the RMSE value between the observed and simulated values at the watershed outlet. The model parameters for the two nitrogen species were simultaneously calibrated using the sum of the RMSE values normalized by the mean observed values (i.e., the normalized RMSE or NRMSE) for NH_4^+ and NO_3^- as a minimized objective function. Similarly, the parameters associated with PO_4^{3-} and Chl *a* were simultaneously calibrated using the sum of the NRMSE values for PO_4^{3-} and Chl *a*, because phosphorous is the most critical limiting nutrient species on the phytoplankton growth (Hecky and Kilham, 1988; Labry et al., 2005; Elser et al., 2011), and thus the model parameters for PO_4^{3-} and Chl *a* have strong mutual influences in the simulation. We did not conduct any intensive calibration for the organics and associated water parameters such as BOD or dissolved oxygen (DO), as we assumed that these parameters have little influence on the Chl *a* simulation results. The study stream was sufficiently shallow (observed water depth ranged from 0.67 to 3.59 m), such that it was always under oxidizing conditions (minimum values of observed and simulated DO were 6.4 mg/L and 4.3 mg/L, respectively) during the study period. Therefore, the variability of the DO may not have a measurable influence on the phytoplankton growth or associated benthic processes such as phosphorous release. For the model calibration, an automatic calibration procedure was applied using the Complex random factorization method (Box, 1965; Guin, 1968; Barco et al., 2008) implemented in MATLAB R2017a (Mathworks, Massachusetts, USA), and coupled with HSPF. Detailed descriptions on the Complex random factorization method and its implementation on MATLAB with repeated running procedure of HSPF can be found in Supplementary material (Appendices A and B).

2.5. Evaluation of model accuracy

Various indicators were used to evaluate the accuracy of the model, including the coefficient of determination (R^2), Nash-Sutcliffe efficiency (NSE), the percent bias (PBIAS), and the RMSE-observation standard deviation ratio (RSR) defined as follows (Moriasi et al., 2007):

$$R^2 = \left(\frac{n\sum_{t=1}^{n} S_t O_t - (\sum_{t=1}^{n} S_t)(\sum_{t=1}^{n} O_t)}{\sqrt{n(\sum_{t=1}^{n} S_t^2) - (\sum_{t=1}^{n} S_t)^2}\sqrt{n(\sum_{t=1}^{n} O_t^2) - (\sum_{t=1}^{n} O_t)^2}} \right)^2 \tag{6}$$

$$NSE = 1 - \frac{\sum_{t=1}^{n} (O_t - S_t)^2}{\sum_{t=1}^{n} (O_t - O_{mean})^2} \tag{7}$$

$$PBIAS = \frac{\sum_{t=1}^{n} (O_t - S_t)}{\sum_{t=1}^{n} O_t} \times 100\% \tag{8}$$

$$RSR = \frac{\sqrt{\sum_{t=1}^{n}(O_t - S_t)^2}}{\sqrt{\sum_{t=1}^{n}(O_t - O_{mean})^2}} = \frac{RMSE}{STDEV_{obs}} \quad (9)$$

where n is the number of data points in the time series, O_t is the observed value at time t, O_{mean} is the mean observed value, and S_t is the simulated value at time t. R^2, derived from Pearson's correlation coefficient, ranges from 0 to 1, and the model is considered more accurate as the value of R^2 approaches 1. In general, a model with an R^2 value greater than 0.5 is considered reasonable (Legates and McCabe, 1999). NSE is one of the most commonly used indicators for judging the accuracy of a hydrological or water quality model (Moriasi et al., 2007). The range of NSE is from $-\infty$ to 1 (Nash and Sutcliffe, 1970), with the greatest accuracy at 1. Percent bias (PBIAS) is the average offset of the simulated values with regard to their observed values in percentage (Gupta et al., 1999). As the PBIAS value approaches 0, the accuracy of the model increases. Positive and negative values of PBIAS indicate underestimation and overestimation biases of the model, respectively (Gupta et al., 1999). The RSR defines the deviation of the model relative to the variation of the measured values. A lower RSR indicates a better model simulation performance (Moriasi et al., 2007). The criteria for the performance ratings ('very good', 'good', 'satisfactory', and 'unsatisfactory') of the PBIAS, RSR, and NSE values on a monthly time step simulation for the flow, sediment, nitrogen, and phosphorous are given in Supplementary Materials (Table S6).

3. Results and discussion

3.1. Parameter sensitivities

The sensitivities and the calibrated values of the model parameters selected for the model calibration are summarized in Tables 1–3. A total of 62 parameters were selected for the model calibration based on their sensitivities for the RMSE values for the flow rate or water quality variables. The remaining 25 model parameters were found to be less sensitive and were therefore not further considered for the model calibration. Table 1 summarizes the results of sensitivity analysis and model calibration for the parameters associated with hydrology, sediment, and water temperature. Among the 10 hydrological parameters, those associated with the recession rates of groundwater and interflow (AGWRC and IRC), the lower zone storage (LZSN), and infiltration capacity of the soil (INFILT) showed greater influence on the simulated stream flow than the other parameters. Although most of the 14 selected sediment parameters (Table 1) were moderately sensitive to the sediment simulation in the stream (S_{LH} > 10), those incorporated in the wash off equation (KSER, JSER, KEIM, and JEIM) and the detachment equation (JRER) showed greater sensitivities compared to the other parameters. In the simulation of water temperature, the temperature of ground (TGRND) and the heat conductance coefficient (KMUD) showed the highest sensitivity. The long wave radiation coefficient (KATRAD) was also significantly influential.

Table 2 summarizes the results of sensitivity analysis and model calibration with respect to ammonia (NH_3 + NH_4^+) and nitrate (NO_3^-). The most sensitive parameter for NH_4^+-N concentration was the unit oxidation rate of total ammonia at 20 °C (KTAM20). The major sensitive parameters for nitrogen species were the concentration of ammonia or nitrate in active groundwater outflow (AOQC), the accumulation rate of ammonia or nitrate in impervious surfaces (IMPLND/ACQOP), the maximum storage of ammonia or nitrate in impervious surfaces (IMPLND/SQOLIM), and the rate of surface runoff of ammonia or nitrate in impervious surfaces (IMPLND/WSQOP). The unit denitrification rate (KNO230) was minimally sensitive for the NO_3-N concentration, because the stream was always under oxidizing conditions during the simulation period.

Table 3 summarizes the results of sensitivity analysis and model calibration with respect to phosphate (PO_4^{3-}) and Chl *a*. The main influencing parameters on the PO_4-P concentration were the wash off potency factors in pervious and impervious land surfaces (POTFW) followed by the upper limit of water temperature for the phytoplankton growth (TALGRH) and the benthic release rate of ortho-phosphate under aerobic conditions (BRPO41). However, the benthic release rate of ortho-phosphate under anaerobic conditions (BROP42) was not considered for calibration because it was insensitive under the oxidizing conditions maintained throughout the study period.

The main influencing parameters on the Chl *a* concentration were the maximal unit growth rate of phytoplankton (MALGR), the rate of phytoplankton settling (PHYSET), and the ratio of Chl *a* content of biomass to phosphorous content (RATCLP). The three temperature parameters (TALGRH, TALGRL, and TALGRM) determining the maximum growth rate of phytoplankton showed moderate or minimal influences on the Chl *a* concentration, probably due to the limitation of the linear temperature-growth formulation of HSPF in simulating the excessive increase in the phytoplankton population at high temperature ranges. The results of the sensitivity rankings of all the model parameters are provided in Supplementary Materials (Tables S7-8).

3.2. Instream calibration of the model

Fig. 4 shows the simulation results of the calibrated model, graphically comparing the observed and simulated flow rates, TW, and concentrations of sediment, NH_4-N, NO_3-N, PO_4-P, and Chl *a*. In the flow and TW simulation, the measured values and simulated values are well fitted. The peak flow rates are also well matched between the observed and simulated values. The simulated sediment concentrations (TSS) closely agreed with the measured values during the calibration period, whereas they tended to be lower than the observed values during the spring seasons, particularly in the validation period with relatively lower precipitations and flow rates compared to the calibration period. The high TSS concentration observed during the spring season that was not properly simulated by the model might be due to the unidentified sources of sediment/soil in streams generated from season-specific rice farming activities in the study area. In Korea, paddy field farming is the typical method of rice growing and requires large quantities of water for irrigation during the spring seasons. This results in discharge of the overflowing irrigation water with entrained pollutants including particles (Song et al., 2013).

The simulated NH_4-N and NO_3-N concentrations closely followed the seasonal patterns of the measured values. Concentrations of the nitrogen species were generally higher during winter seasons, which was coincidence with the seasonality of the effluent TN concentrations of the wastewater treatment plants. The concentration of NH_4-N was remarkably higher during the winter season than during non-winter seasons with NH_4-N concentration maintained at a very low level ($<$ 0.05 mg/L). In contrast, the seasonality of NO_3-N concentration was less significant, and generally higher than NH_4-N concentration throughout all seasons. In the HSPF model, the difference in the seasonal variation between NH_4-N and NO_3-N was reproduced by allowing monthly variable concentration parameters in the active groundwater (AOQC); the pollutant accumulation and wash off coefficients in the catchment were assumed to be temporarily constant and thus any possible seasonality in atmospheric deposition were not considered in the simulation. The calibration results showed that nitrate concentration in the active groundwater (AOQC) was maintained between 2.1–3.5 mg/L, functioning as an effective supplier of nitrate to the stream. This result is supported by the nitrate contamination of the groundwater frequently reported in Asian agricultural areas including Korea (Jeon et al., 2011; Liu et al., 2017). By comparing the simulation results with and without phytoplankton processes, the seasonality and concentrations of nitrogen species were not found to be significantly affected by the time-varying phytoplankton growth rate because nitrogen generally was less limited for the phytoplankton growth in the stream water of the study site (average TN/TP molar ratio of the

Table 2
Sensitivities and calibrated values of the model parameters selected for the model calibration with respect to nitrogen species.

Parameter			Description	Range		LH-OAT sensitivity to RMSE (S_{LH})		Calibrated value	Remarks
Group	Name	Unit		min	max	NH_4^+-N concentration	NO_3^--N concentration		
Ammonia (9 parameters)									
PERLND	ACQOP	lb/ac·day	Rate of accumulation of total ammonia in pervious surfaces	0	0.15	1.543	0.018	0.134	
PERLND	SQOLIM	lb/ac	Maximum storage of total ammonia in pervious surfaces	0	2	0.611	0.008	0.285	
PERLND	WSQOP	in/hr	Rate (per hour) of surface runoff that will remove 90% of stored total ammonia in pervious surfaces	0.01	10	1.090	0.018	1.159	
PERLND	IOQC	lb/ft^3	Concentration of total ammonia in interflow outflow	0	5E-5	0.223	0.010	0	
PERLND	AOQC	lb/ft^3	Concentration of total ammonia in active groundwater outflow	0	3.0E-4	15.636	1.014	0 – 2.5E-4	Calibrated for each month
IMPLND	ACQOP	lb/ac·day	Rate of accumulation of total ammonia in impervious surfaces	0	15	58.810	1.810	0.094	
IMPLND	SQOLIM	lb/ac	Maximum storage of total ammonia in impervious surfaces	0	150	161.309	5.204	0.155	
IMPLND	WSQOP	in/hr	Rate (per hour) of surface runoff that will remove 90% of stored total ammonia in impervious surfaces	0.01	10	145.478	9.753	3.114	
RCHRES	KTAM20	1/hr	Unit oxidation rate of total ammonia at 20 °C	0.001	0.5	178.556	8.606	0.015	
Nitrate(9 parameters)									
PERLND	ACQOP	lb/ac·day	Rate of accumulation of nitrate in pervious surfaces	0	0.15	–	0.242	1.024	
PERLND	SQOLIM	lb/ac	Maximum storage of nitrate in pervious surfaces	0	150	–	0.076	12.909	
PERLND	WSQOP	in/hr	Rate (per hour) of surface runoff that will remove 90% of stored nitrate in pervious surfaces	0.01	100	–	0.221	13.284	
PERLND	IOQC	lb/ft^3	Concentration of nitrate in interflow outflow	0	5E-5	–	0.044	2.45E-5	
PERLND	AOQC	lb/ft^3	Concentration of nitrate in active groundwater outflow	0	6.6E-4	–	116.998	1.3E-4 – 2.2E-4	Calibrated for each month
IMPLND	ACQOP	lb/ac·day	Rate of accumulation of nitrate in impervious surfaces	0	15	–	30.540	0.012	
IMPLND	SQOLIM	lb/ac	Maximum storage of nitrate in impervious surfaces	0	150	–	70.776	13.314	
IMPLND	WSQOP	in/hr	Rate (per hour) of surface runoff that will remove 90% of stored nitrate in impervious surfaces	0	10	–	61.045	0.794	
RCHRES	KNO320	1/hr	Unit denitrification rate of nitrate at 20 °C	0.001	0.4	–	0.961	0.015	

Table 3
Sensitivities and calibrated values of the model parameters selected for the model calibration with respect to phosphate and Chl *a*.

Parameter			Description	Range		LH-OAT sensitivity to RMSE (S_{LH})		Calibrated value	Remarks
Group	Name	Unit		min	max	PO_4^{3-} -P concentration	Chl *a* concentration		
Phosphate (3 parameters)									
PERLND	POTFW	–	Washoff potency factor in pervious surfaces	0.007	44	0.003-101.738	0.000-0.052	0.007-32.527	Calibrated for each land-use class
IMPLND	POTFW	–	Washoff potency factor in impervious surfaces	6.4	858	52.738	0.331	6.4	
RCHRES	BRPO41	$mg/m^2/hr$	Benthal release rate of ortho-phosphate under aerobic conditions	0	1	15.146	2.003	0	
Phytoplankton (11 parameters)									
PLANK	RATCLP	–	Ratio of Chl *a* content of biomass to phosphorus content	0.01	2	0.027	3.647	1.370	
PLANK	EXTB	1/ft	Base extinction coefficient for light	0.001	1	0.159	0.085	0.175	
PLANK	MALGR	1/hr	Maximal unit algal growth rate for phytoplankton	0.008	0.3	1.804	5.448	0.229	
PLANK	CMMLT	ly/min	Michaelis-Menten constant for light limited growth for phytoplankton	0.012	0.036	0.437	0.320	0.029	
PLANK	CMMN	mg/L	Nitrate Michaelis-Menten constant for nitrogen limited growth for phytoplankton	0.001	0.1	0.039	0.193	0.059	
PLANK	CMMP	mg/L	Phosphate Michaelis-Menten constant for phosphorus limited growth for phytoplankton	0.0005	0.08	0.697	2.574	0.029	
PLANK	TALGRH	°F	Temperature above which phytoplankton growth ceases	50	90	33.141	2.915	86.739	
PLANK	TALGRL	°F	Temperature above which phytoplankton growth ceases	−120	90	7.411	0.787	61.275	
PLANK	TALGRM	°F	Temperature below which phytoplankton growth is retarded	32	90	1.599	2.466	79.679	
PLANK	ALR20	1/hr	Phytoplankton unit respiration rate at 20 °C	0.002	0.006	0.535	0.189	0.003	
PLANK	PHYSET	ft/hr	Rate of phytoplankton settling	0	0.07	0.105	4.019	0.000	

observed data = 75 > 16, the Redfield ratio).

The observed and simulated concentrations of PO_4-P were generally higher during winter seasons than non-winter seasons. However, the seasonality of the PO_4-P concentration was less profound in the observation than in the simulation; the simulated PO_4-P concentration was near zero during summer seasons, whereas the observed PO_4-P concentration was constantly maintained above the detection limit (~0.02-0.05 mg P/L) during the same seasons. This difference in the background level of PO_4-P between the observation and simulation might be caused by the background phosphorous sources, such as atmospheric deposition and soils/rocks weathering, which were not considered in the model (Gardner, 1990; Tipping et al., 2014). The influences of active groundwater on the phosphorous concentration in streams can be considered insignificant because of the low mobility of phosphorous in the groundwater (Holman et al., 2008). Therefore, the surface runoff driven by precipitation can be the major factor affecting the temporal variation of the PO_4-P inputs to the streams. However, the larger input of phosphorous during the summer season might not always result in a high instream concentration of phosphorous, because phosphorous introduced into streams can be largely consumed by phytoplankton at higher temperature conditions during the season.

The original HSPF model was used to simulate the seasonal trend of Chl *a*, predicting higher concentrations during summer but the Chl *a* concentration was generally underestimated throughout the study period. HSPF simulates only one group of phytoplankton species using a linear temperature-growth formulation; this becomes its intrinsic limitation in simulating varying growth tendencies of diverse phytoplankton species with different optimal growth temperatures possibly present in surface water bodies. The model failed to simulate the base level of Chl *a* during the non-summer seasons and the excess level of Chl *a* during the summer seasons.

3.3. Improvements on the Chl a simulation

Fig. 5 compares the observed and simulated concentrations of PO_4-P and Chl *a* for the three different equations to describe the temperature-growth relationship of the phytoplankton: the original linear equation and two modifications into quadratic and exponential equations. In this study, we focused on the accuracy of the model in simulating the excessively high concentrations of Chl *a* occurring in the summer seasons, which is the primary management target for water quality managers. As shown in Fig. 5, the exponential equation better simulates the patterns of Chl *a* that substantially increase during the summer seasons. Table 4 summarizes the performance of the model in predicting the trophic states of the water, based on the eutrophic state criteria, Chl $a \geq 20$ μg/L (Carlson, 1996). The linear and exponential equations showed the same prediction accuracy of 84% and 92% for the eutrophic and oligo-mesotrophic states, respectively, in calibration, while the exponential equation outperformed the linear equation in predicting both trophic states. The performance of quadratic equation was always less than that of linear and exponential equations. The exponential equation was especially useful in simulating the summer seasons with high concentrations of Chl *a*.

3.4. Performance of the calibrated model

Table 5 shows a summary of the four different accuracy indicators computed for different constituents simulated by the HSPF model. Similarly to prior studies (He and Hogue, 2012; Stern et al., 2016), the model showed relatively good performance for flow and TW based on all the indicators being within their satisfactory ranges ($R^2 > 0.7$, NSE > 0.7, PBIAS ~ 15.71–25.14%, and PSR < 0.53). For the sediment, all indicator values of the calibration period were satisfactory or better, while the accuracy indicators of the validation period were relatively poor except for PBIAS. The values of PBIAS for all variables were within the satisfactory performance ranges in both the calibration

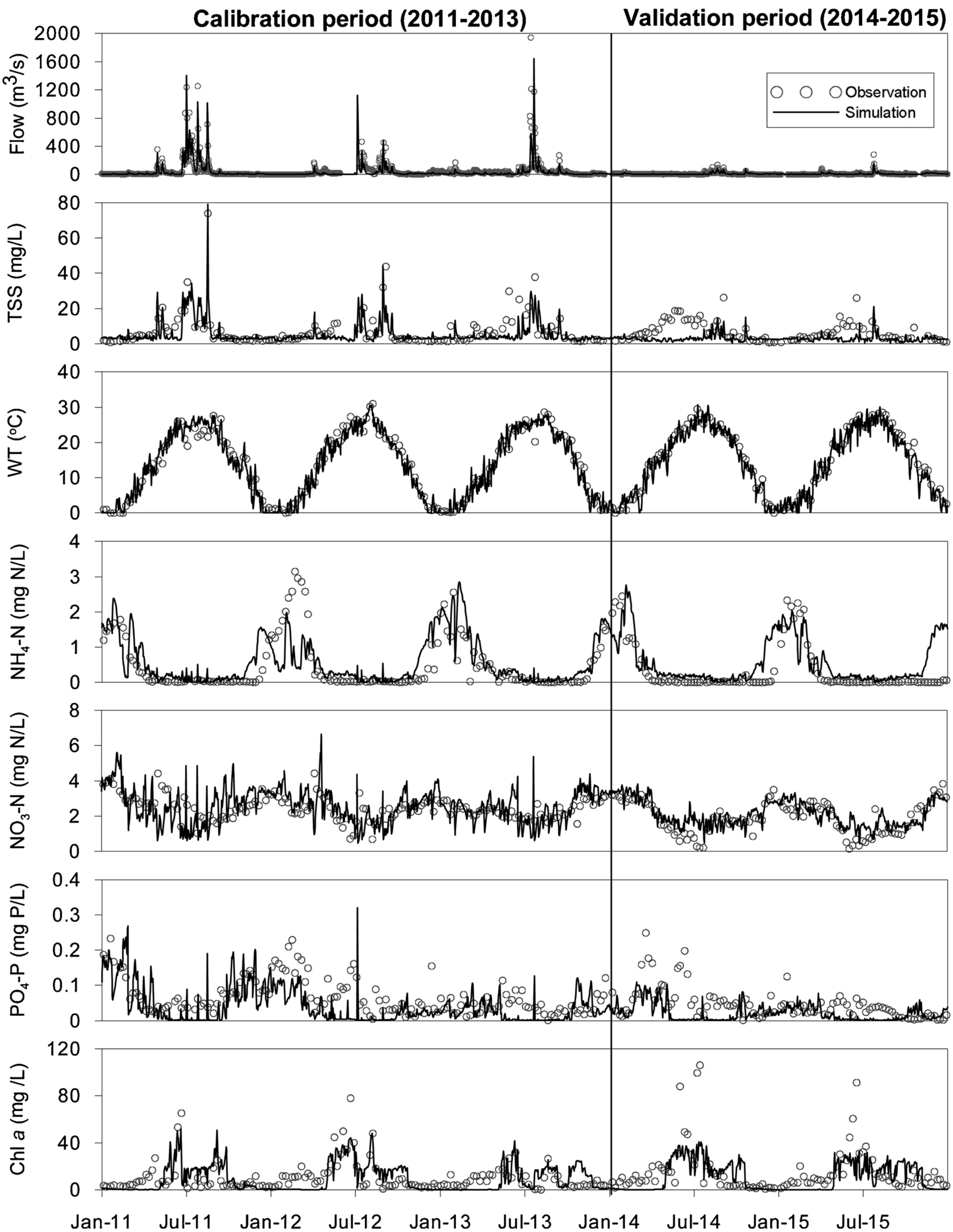

Fig. 4. Observed and simulated flow, water temperature, and constituents during calibration and validation periods.

and validation periods. Several previous studies reporting the values of R^2 or NSE on the sediment could be found in the literature (Table S9), ranging from 0.37 to 0.94 for R^2 from daily or monthly calibration, and from -3.51 to 0.92 for NSE from monthly calibration (Saleh et al., 2000; Santhi et al., 2001; Saleh and Du, 2004; Bracmort et al., 2006; Stern et al., 2016; Ahn and Kim, 2016). No reported values of daily basis NSE for sediment were found in the literature. While the accuracy of the sediment simulation of this study was comparable to that of the previous studies, the accuracy for the validation period was relatively low. The relatively low precipitation in the validation period resulted in low simulated TSS concentrations in the stream, increasing the deviation from the high TSS concentration observed in the spring seasons, may be a result from the discharge of the paddy fields, as mentioned previously (see Fig. 3).

The values of R^2, NSE, and RSR for nitrogen species, PO_4-P, and Chl *a* were generally within the ranges of unsatisfactory performance ratings, while the performance ratings based on PBIAS were satisfactory or better for all constituents and simulation periods (calibration and validation). However, the indicator values in this study were comparable to those in the previous studies (Table S9), considering that the temporal resolutions (5–8 days) used in this study were finer than those used in most of the previous studies in which monthly calibrations were

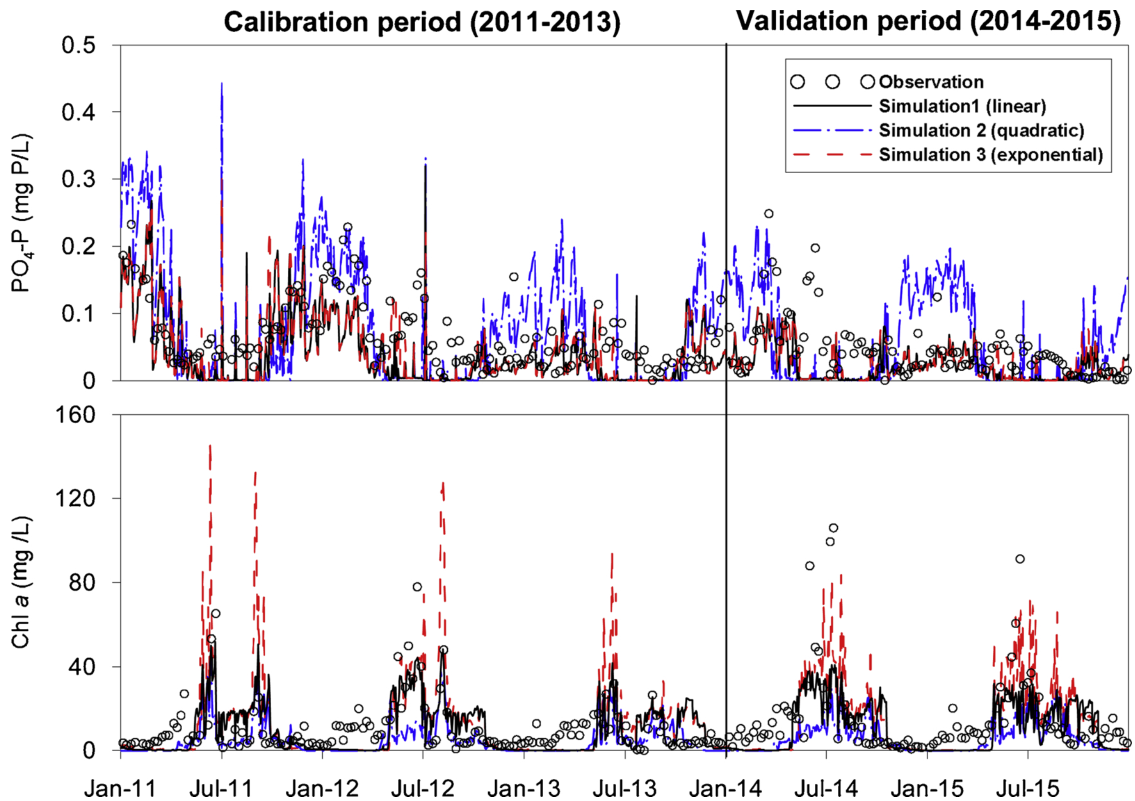

Fig. 5. Comparison of PO_4-P and Chl *a* concentrations simulated by the three growth-temperature formulations of phytoplankton in HSPF.

used. When the indicator values were recalculated using monthly averaged data (the values in the parenthesis in Table 5), the accuracies generally improved. Furthermore, most of the previous studies rated the model performance targeting lumped sum variables (*e.g.* TN, TP, or a sum of organic N and NO_3-N), which may generally result in better model performance ratings compared to this study targeting a single species, (*e.g.* NO_3-N or PO_4-P) (Moriasi et al., 2007). No previous studies reported the accuracy indicators of NH_4^+ and Chl *a*.

As show in Table 5, the exponential temperature-growth model was slightly better in simulating the Chl *a* concentration when considering the values of R^2 relatively high in both the calibration and validation steps. However, the linear temperature-growth model outperformed the exponential temperature-growth model in the calibration step, based on the NSE values: the monthly values of NSE were -0.37 and 0.29 for the linear and exponential temperature-growth models, respectively. However, it should be noted that the exponential temperature-growth model could be more valuable for simulating the excess growth of phytoplankton during summer seasons.

4. Conclusions

This study offered an improved accuracy of the instream Chl *a* simulation in the HSPF model using an automatic calibration and modification on the Chl *a* calculation module. Important model parameters were selected from senstivity analyses and then automatically calibrated. From this study, the following conclusions are made:

1 Sets of crucial HSPF model parameters for flow, water temperature, sediment, ionic nutrient species and Chl *a* were drawn through the LH-OAT sensitivity analysis, which were selected as the parameters to be automatically calibrated by the Complex random factorization algorithm. The suggested crucial parameter sets can be used as guidance for other watershed modeling applications with different site-specific conditions..
2 The Complex random factorization algorithm was applied in a stepwise manner for different parameter groups and was effective in automatically calibrating the HSPF model, which is intrinsically difficult and thus no attempts have been made in pervious studies.
3 The performance ratings of the calibrated model with 5–8 day

Table 4
Model performance in predicting the trophic state.

Phytoplankton growth-temperature formulation		Eutrophic cases (Chl *a* ≥ 20 μg/L)			Oligo-mesotrophic cases (Chl *a* < 20 μg/L)		
		Success	Failure	Total	Success	Failure	Total
Linear (original)	Calibration	16 (84%)	3 (16%)	19	120 (92%)	11 (8%)	131
	Validation	12 (52%)	11 (48%)	23	86 (84%)	16 (16%)	102
Quadratic	Calibration	6 (32%)	13 (68%)	19	126 (96%)	5 (4%)	131
	Validation	3 (13%)	20 (87%)	23	98 (96%)	4 (4%)	102
Exponential	Calibration	16 (84%)	3 (16%)	19	120 (92%)	11 (8%)	131
	Validation	18 (78%)	5 (22%)	23	89 (87%)	13 (13%)	102

Note: Numbers in parentheses are percentage of the cases.

Table 5
Summary of the accuracy indicator values of the HSPF model in this study.

Variable (data resolution)	Phytoplankton-temperature formulation	Simulation type	Accuracy Indicators[a]			
			R^2	NSE	PBIAS (%)	RSR
Flow (daily)	–	Calibration	**0.75 (0.91)**	**0.74 (0.87)**	**24.04** (25.14)	**0.51 (0.36)**
		Validation	**0.77 (0.76)**	**0.73 (0.72)**	**15.71 (16.05)**	**0.16 (0.53)**
Sediment (5-8days)	–	Calibration	**0.71 (0.68)**	**0.68 (0.61)**	**19.95 (22.03)**	**0.13 (0.63)**
		Validation	0.10 (0.06)	−0.38 (-0.50)	**54.76 (52.24)**	1.17 (1.23)
Water Temp (5-8days)	–	Calibration	**0.96 (0.97)**	**0.96 (0.97)**	**1.62 (1.44)**	**0.22 (0.17)**
		Validation	**0.96 (0.98)**	**0.96 (0.97)**	**3.09 (3.16)**	**0.05 (0.17)**
NH_4-N (5-8days)	–	Calibration	0.41(**0.54**)	0.32(**0.50**)	**−14.95(-12.95)**	0.82(0.71)
		Validation	0.46(**0.51**)	0.28(0.39)	**−52.55(-47.26)**	0.85(0.78)
NO_3-N (5-8days)	–	Calibration	0.17(0.44)	−1.05(0.03)	**−2.45(-0.71)**	1.43(0.98)
		Validation	**0.63(0.80)**	**0.61(0.77)**	**−6.45(-7.08)**	**0.63(0.48)**
PO_4-P (5-8days)	Original	Calibration	0.24 (0.48)	−0.45 (0.11)	**36.46 (37.99)**	1.21 (0.94)
		Validation	0.06 (0.19)	−0.35 (-0.28)	**53.34 (54.98)**	1.16 (1.13)
	Quadratic	Calibration	0.28 (0.42)	−1.31 (-0.74)	**−11.60 (-12.96)**	1.52 (1.32)
		Validation	2E-4 (8E-6)	−2.15 (-2.43)	**−18.06 (-19.95)**	3.15 (1.85)
	Exponential	Calibration	0.26 (**0.51**)	−0.32 (0.21)	**33.85 (34.44)**	1.15 (0.89)
		Validation	0.04 (0.18)	−0.34 (-0.18)	**47.43 (47.93)**	1.16 (1.08)
Chl *a* (5-8days)	Original	Calibration	0.36 (0.43)	0.22 (0.29)	**6.60 (9.19)**	0.88 (0.84)
		Validation	0.25 (0.41)	0.18 (0.34)	**33.44 (28.21)**	0.88 (0.81)
	Quadratic	Calibration	0.26 (0.30)	0.05 (-0.002)	**50.71 (52.16)**	0.97 (1.00)
		Validation	0.16 (0.37)	−0.07 (-0.02)	**61.47 (60.21)**	1.03 (1.01)
	Exponential	Calibration	0.35 (0.39)	−0.62 (-0.37)	**−20.45 (-21.05)**	1.27 (1.17)
		Validation	0.36 (**0.61**)	0.28 (**0.58**)	**9.83 (6.15)**	0.85 (**0.65**)

[a] Values in the parentheses are the indicator values of the month-average values of the variables. Bold face values indicate that the accuracy of the model can be considered satisfactory (acceptable) or better. The BIASP criteria for Chl a were assumed the same as those for nutrients.

interval time series data were better than or equal to the 'satisfactory' levels, for individual ionic nutrient species and Chl *a*. The obtained performance ratings were fairly comparable with those in the literature, which were mostly based on monthly calibration or based on gross nutrient parameters such as total nitrogen and total phosphorous. No Chl *a* calibration reports were found in the existing HSPF modeling literature.

4 Among the three formulations of the temperature-growth relationship of phytoplankton, the exponential equation was more efficient than the original linear equation or the quadratic equation in simulating excess growth of phytoplankton during summer seasons.

This study demonstrated how the extremely large number of model parameters of a sophisticated watershed model such as HSPF can be managed to ensure the model's validity. It also demonstrated how the critical modification on the phytoplankton growth formulation can improve the Chl *a* simulation. As a future study, coupling such model with remote sensing of Chl *a* could improve our understanding the dynamics of algal blooms. The improved Chl *a* simulation using the approach suggested in this study, coupled with remote sensing modeling in the future, should be useful for early warning of algal blooms and help decision makers in developing proactive management plans.

Acknowledgements

This work was supported by the Research program of Dongguk University, 2018, and grants from the National Research Foundation (NRF) of Korea, funded by the Korea government (No. 2015R1D1A1A01056753 and No. 2015H1A2A1034045).

Appendix A. Supplementary data

Supplementary material related to this article can be found, in the online version, at doi:https://doi.org/10.1016/j.ecolmodel.2019.108835.

References

Abdulla, F., Eshtawi, T., Assaf, H., 2007. Assessment of the impact of potential climate change on the water balance of a semi-arid watershed. Water Resour. Manag. 23 (10), 2051–2068.

Ahn, S.R., Kim, S.J., 2016. The Effect of Rice Straw Mulching and No-Tillage Practice in Upland Crop Areas on Nonpoint-Source Pollution Loads Based on HSPF. Water 8 (3), 106.

Alberk, M., Öğütveren, Ü.B., Albek, E., 2004. Hydrological modeling of Seydi Suyu watershed (Turkey) with HSPF. J. Hydrol. 285 (1-4), 260–271.

Auer, M.T., Kieser, M.S., Canale, R.P., 1986. Identification of critical nutrient levels through field verification of models for phosphorus and phytoplankton growth. Can. J. Fish. Aquat. Sci. 43 (2), 379–388.

Barco, J., Wong, K.M., Stenstrom, M.K., 2008. Automatic calibration of the U.S. EPA SWMM model for a large urban catchment. J. Hydraulics, ASCE 134 (4), 466–473.

Bicknell, B.R., Imhoff, J.C., Kittle, J.L., Jobes, T.H., Donigian Jr., A.S., 2001. Hydrological Simulation Program—FORTRAN (HSPF). User's Manual for Release 12; EPA Environmental Research Laboratory and Office of Surface Water Geological Survey: Athens. GA, USA; Reston, VA, USA.

Boyer, J.N., Kelble, C.R., Ortner, P.B., Rudnick, D.T., 2009. Phytoplankton bloom status:Chlorophyll *a* biomass as an indicator of water quality condition in the southern estuaries of Florida. USA. Ecol. indicators 9 (6), S65–S67.

Bowie, G.L, Mills, W.B., Porcella, D.B., Campbell, C.L., Pagenkopf, J.R., Rupp, G.L., Johnson, K.M., Chan, P.W.H., and Gherini, S.A., 19850. Rates, constants, and kinetics formulations in surface water quality modelling (second edition). EPA/600/3-85/040, U.S. Environmental Protection Agency, Athens, Georgia, USA.

Bracmort, K.S., Arabi, M., Frankenberger, J.R., Engel, B.A., Arnold, J.G., 2006. Modeling long-term water quality impact of structural BMPS. Trans. ASAE 49 (2), 367–384.

Box, M.J., 1965. A new method of constrained optimization and a comparison with other method. Comput. J. 8 (1), 42–52.

Carlson, R.E., 1996. A coordinator's guide to Volunteer Lake monitoring methods. North Am. Lake Manage. Soc. 96.

Chen, D., Lu, j., Wang, H., Shen, Y., Gong, D., 2011. Combined inverse modeling approach and load duration curve method for variable nitrogen total maximum daily load development in an agricultural watershed. Environ. Sci. Pollut. Res. 18, 1405–1413.

Debela, B., Srinvasa, R., Parlange, J.-Y., 2006. Coupling upland watershed and downstream waterbody hydrodynamic and water quality models (SWAT and CE-QUAL-W2) for better water resources management in complex river basins. Environ. Model. Assess. 13 (1), 135–153.

Elser, J.J., Marzolf, E.R., Goldman, C.R., 2011. Phosphorus and nitrogen limitation of phytoplankton growth in the freshwaters of North America: a review and critique of experimental enrichments. Can. J. Fish. Aquat. Sci. 47 (78), 1468–1477.

Fonseca, A., Botelho, C., Boaventura, R.A.R., Vilar, V.J.P., 2014. Integrated hydrological and water quality model for river management: a case study on Lena River. Sci. Total Environ. 485–486, 474–489.

Gardner, L.R., 1990. The role of rock weathering in the phosphorus budget of terrestrial watersheds. Biogeochemistry 11, 97–110.

Guin, J.A., 1968. Modification of the Complex method of constrained optimization. Comput. J. 10 (4), 416–417.

Gupta, H.V., Sorooshian, S., Yapo, P.O., 1999. Status of automatic calibration for hydrologic models: comparison with multilevel expert calibration. J. Hydrol. Eng. 4 (2), 135–143.
He, M., Hogue, T.S., 2012. Integration hydrological modeling and land use projections for evaluation of hydrologic response and regional water supply impacts in semi-arid environmental. Environ. Earth Sci. 65 (6), 1671–1685.
Hecky, R.E., Kilham, P., 1988. Nutrient limitation of phytoplankton in freshwater and marine environments: a review of recent evidence on the effects of enrichment. Limnol. Oceanogr. 33 (4part2), 796–822.
Holman, I.P., Whelen, M.J., Howden, N.J.K., Bellamy, P.H., Willby, N.J., Rivas-Casado, M., McConvey, P., 2008. Phosphorus in groundwater-an overlooked contributor eutrophication? Hydrolocigal Processes 22 (26), 5121–5127.
Hutorowicz, A., Pasztaleniec, A., 2014. Phytoplankton metric of ecological status assessment for polish lakes and its performance along nutrient gradients. Pol. J. Ecol. 62 (3), 525–540.
Jeon, S.R., Jung, S.K., Lee, Y.U., Chung, J.I., 2011. Hydrogeochemical characteristics and estimation of nitrate contamination sources of groundwater in the Sunchang area. Korea. J. Geol. Soc. Korea 47 (2), 185–197.
Jha, M.K., Wolter, C.F., Schilling, K.E., Gassman, P.W., 2010. Assessment of total maximum daily load implementation strategies for nitrate impairment of the Raccoon River. Iowa. J. Environ. Quality 39 (4), 1317–1327.
Kang, M.G., An, I.S., Kim, Y., 2005. Survey of the secondary effluents from municipal wastewater treatment plants in Korea. J. Korean Soc.Water Quality 21 (2), 158–168.
Labry, C., Delmas, D., Herbland, A., 2005. Phytoplankton and bacterial alkaline phosphatase activities in relation to phosphate and DOP availability within the Gironde plume waters (Bay of Biscay). J. Exp. Mar. Biol. Ecol. 318 (2), 213–225.
LaWare, P., Rifai, H.S., 2006. Modeling fecal coliform contamination in the Rio Grande. J. Am. Water Resour. Assoc. 42 (2), 337–356.
Legates, D.R., McCabe, G.J., 1999. Evaluating the use of "goodness-of-fit" measures in hydrologic and hydro climatic model validation. Can. Water Resour. 35 (1), 233–241.
Lee, J.H.W., Hodgkiss, I.J., Wong, K.T.M., Lam, I.H.Y., 2005. Real time observations of coastal algal blooms by an early warning system. Estuar. Coast. Shelf Sci. 65 (1-2), 172–190.
Lee, S.J., Lee, S.E., Kim, S.H., Park, H.K., Park, S.J., Yum, K.T., 2011. Examination of Critical Factors Related to Summer Chlorophyll *a* Concentration in the Sueo Dam Reservoir, Republic of Korea. Environ. Eng. Sci. 29 (6), 502–510.
Liu, J., Jiang, L.H., Zhang, C.J., Li, P., Zhao, T.K., 2017. Nitrate-nitrogen contamination in groundwater: spatiotemporal variation and driving factors under cropland in Shandong Province, China. The 3rd International Conference in Water Resource and Environment. IOP Conf. Series: Earth and Environ. Sci. 82, 012059.
Loucks, D.P., Van Beek, E., 2005. Water resources systems planning and management. An Introduction to Methods. Models and Applications. Unesco Publishing.
Moriasi, D.N., Arnold, J.G., Van Liew, M.W., Bingner, R.L., Harmel, R.D., Veith, T.L., 2007. Model evaluation guidelines for systematic quantification of accuracy in watershed simulation. Trans. Asabe 50 (3), 885–900.
Nash, J.E., Sutcliffe, J.V., 1970. River flow forecasting through conceptual models part 1 – a discussion of principles. J. Hydrol. (Amst) 10 (3), 282–290.
Paerl, H.W., Valdes, L.M., Pinckney, J.L., Piehler, M.F., Dyble, J., Moisander, P.H., 2003. Phytoplankton photopigments as indicators of estuarine and coastal eutrophication. BioScinece 53 (10), 953–964.
Park, J.C., Lee, J.K., Lee, S.P., Seong, J.U., 2013. Effects of Gumi City sewage treatment effluent in the downstream nutrient matter: comparison of daily loading. J. Environ. Sci.Int. 22 (12), 1643–1650.
Park, Y., Cho, K.H., Kang, J.H., Lee, S.W., Kim, J.H., 2014. Developing a flow control strategy to reduce nutrient load in a reclaimed multi-reservoir system using a 2D hydrodynamic and water quality model. Sci. Total Environ. 466-467, 871–880.
Saleh, A., Arnold, J.G., Gassman, P.W., Hauk, L.M., Rosenthal, W.D., Williams, J.R., MacFarland, A.M.S., 2000. Application of SWAT for the upper north bosque river watershed. Trans. ASAE 43 (5), 1077–1087.
Saleh, A., Du, B., 2004. Evaluation of SWAT and HSPF within BASINS program for the upper North Bosque River watershed in central Texas. Trans. ASAE 47 (4), 1039–1049.
Santhi, C., Arnold, J.G., Williams, J.R., Dugas, W.A., Srinivasan, R., Hauck, L.M., 2001. Validation of the SWAT model on a large river basin with point and nonpoint sources. J. Am. Water Resour. Assoc. 37 (5), 1169–1188.
Sherk, G.W., Linker, L.C., 2013. Development and application of the 2010 chesapeake bay watershed total maximum daily load model. J. Am. Water Resour. Assoc. 49 (5), 1042–1056.
Singh, V.P., Frevert, D.K., 2006. Watershed Models. Boca Raton, Taylor & Francis.
Song, J.H., Kang, M.S., Song, I., Hwang, S.H., Park, J.J., Jun, S.M., Kim, K.U., Jang, J.R., 2013. Analysis of nutrient load balance in the reservoir irrigated paddy block. J. Korean Soc. Agric. Eng. 55 (6), 167–175.
Stern, M., Flint, L., Minear, J., Flint, A., Wright, S., 2016. Characterizing changes in streamflow and sediment supply in the Sacramento River Basin, California, Using hydrological simulation program—FORTRAN (HSPF). Water 8 (10), 432.
Smith, V.H., Tilman, G.D., Nekola, J.C., 1999. Eutrophication: impacts of excess nutrient inputs on freshwater, marine, and terrestrial ecosystems. Environ. Pollut. 100 (1-3), 179–196.
Tim, U.S., 1995. Emerging technologies for hydrologic and water quality modeling research. Trans. ASAE 39 (2), 465–476.
Tipping, E., Benham, S., Boyle, J.F., Crow, P., Davies, J., Fischer, U., Guyatt, H., Helliwell, R., Jackson-Blake, L., Lawlor, A.J., Monteith, D.T., Rowe, E.C., Toberman, H., 2014. Atmospheric deposition of phosphorus to land and freshwater. Environ. Sci.: Processes Impacts 16, 1608–1617.
US EPA, 2000. BASINS Technical Note 6; Estimating Hydrology and Hydraulic Parameters for HSPF. EPA-823-R00-012. U.S. Environmental Protection Agency, Office of Water, Washington, DC. USA.
USEPA, 2013. Better Assessment Science Integrating Point and Nonpoint Sources (BASINS) Version 4.1, EPA-823-B-13-001.
van Griensven, A., Meixner, T., Grunwald, S., Bishop, T., Diluzio, M., Srinivasan, R., 2006. A global sensitivity analysis tool for the parameters of multi-variable catchment models. J. Hydrol. (Amst) 342 (1-4), 10–23.
Wagner, T., Erickson, L.E., 2017. Sustainable management of eutrophic lakes and reservoirs. Scientific Research Publishing 8 (4), 436–463.